Structures 75 (2025) 108768

Contents lists available at ScienceDirect

Structures

journal homepage: www.elsevier.com/locate/structures

Compressive behaviour of stub composite columns with stainless steel square outer tubes and recycled aggregate concrete

Xianghe Dai [a,*], Kan Zhou [b], Jie Yang [c]

[a] Faculty of Engineering and Digital Technologies, University of Bradford, UK
[b] School of Built Environment, Engineering and Computing, Leeds Beckett University, Leeds, UK
[c] Global Research and Development, ArcelorMittal, Luxembourg

ARTICLE INFO

Keywords:
Stainless steel composite column
Recycled aggregate concrete
Square section
Axial compressive capacity
Experiment
Numerical simulation
Parametric study

ABSTRACT

In recent years, stainless steel has been increasingly used in construction practices due to its appealing appearance, high strength, and satisfactory corrosion resistance, which contribute to a long lifespan. Stainless steel hollow sections are extensively employed as structural members. This paper investigates the axial compressive behaviour of stub composite columns with stainless steel square outer tubes and different aggregate concrete. An experimental programme involving 12 specimens was conducted to study the effects of cross-sectional dimensions, and the types and sizes of coarse aggregates. The load-bearing capacity and failure modes of the specimens were recorded and analysed. A comprehensive parametric study was performed, examining three stainless steel types, different cross-sectional dimensions and two concrete grades. The result showed that while the types and sizes of coarse aggregates influenced the compressive strength of concrete, aggregate sizes of 10 mm and 20 mm did not significantly impact the axial compressive strength of concrete-filled stainless steel composite columns. The axial compressive capacity of concrete-filled stainless steel columns was significantly influenced by the type of stainless steel and the cross-sectional width-to-wall thickness ratio. A simple formula is proposed to predict the cross-sectional compressive capacity of concrete-filled stainless steel columns.

1. Introduction

Concrete-filled steel tubular (CFST) columns are extensively used in modern construction worldwide, particularly in high-rise buildings, industrial plants, bridge piers, public utility posts such as subway station columns, and pile foundations etc. due to their enhanced load-bearing capacity, high ductility, excellent energy dissipation and fire resistance. Steel-concrete composite tubular columns utilise the favourable properties of both constituent materials and the tubes come in circular, square, rectangular, elliptical, and other specially designed cross-sectional shapes. The behaviour of composite columns, particularly CFST columns, has been investigated extensively [1,2].

Recycled aggregate concrete has been advocated in the construction sector worldwide [3]. It reduces the exploitation of natural resources as well as construction and demolition waste, contributing to net-zero carbon targets and the transition from a linear to a circular economy, bringing social, environmental, and economic benefits to all stakeholders across the value chain. Even though recycled aggregates may present drawbacks such as higher shrinkage and creep, increased porosity, high water absorption, and reduced concrete strength, the structural performance can potentially be improved through measures such as limiting the replacement ratio, treating the recycled aggregates, or incorporating them in composite steel-concrete members [4–10]. Notably, existing research, primarily focused on composite columns using carbon steel tubes, has shown that the mechanical properties of such composite columns can be comparable to those of concrete made with natural aggregates. However, studies on the combined used of recycled aggregate concrete and stainless steel tubes remains limited [10].

Stainless steel offers high strength, durability, corrosion resistance and fire resistance, resulting in a longer lifespan and reduced environmental impact, in addition to its aesthetic advantage. The mechanical properties of stainless steel [11], its applications in composite columns with conventional concrete, and the corresponding design methods have been studied [12–16]. It has been found that the bond strength between the stainless steel tube and the infilled concrete decreases due to the

* Corresponding author.
E-mail address: x.dai@Bradford.ac.uk (X. Dai).

https://doi.org/10.1016/j.istruc.2025.108768
Received 31 October 2024; Received in revised form 19 March 2025; Accepted 24 March 2025
Available online 2 April 2025

Table 1
Summary of specimen dimensions, concrete strengths and test results.

Specimen *ID*	L(mm)	B (mm)	t (mm)	B/t	f_{cu} (N/mm^2 at 28 days)	f_{cu} (N/mm^2, at test date)	N_{max} (kN)	Shortening at N_{max} (mm)
S_300 × 100 × 5-Granite 10	300.1	100.1	5.0	20.0	31.2	33.0	1362.8	6.3
S_300 × 100 × 2-Granite 10	300.0	100.0	2.0	49.5	31.2	33.0	594.9	2.1
S_180 × 60 × 3-Granite 10	185.0	60.0	3.1	19.7	31.2	33.0	709.1	4.8
S_300 × 100 × 5-Recycled 10	300.0	100.0	5.0	20.1	30.0	30.1	1308.5	6.6
S_300 × 100 × 2-Recycled 10	300.0	99.9	2.0	49.9	30.0	30.1	583.4	2.1
S_180 × 60 × 3-Recycled 10	185.1	60.0	3.0	19.8	30.0	30.1	682.1	5.0
S_300 × 100 × 5-Granite 20	300.0	100.0	5.1	19.7	36.3	38.2	1374.7	7.0
S_300 × 100 × 2-Granite 20	300.1	100.1	2.0	49.5	36.3	38.2	611.2	1.9
S_180 × 60 × 3-Granite 20	185.0	60.0	3.0	20.0	36.3	38.2	737.8	5.0
S_300 × 100 × 5-Gravel 20	300.2	100.0	5.0	19.9	36.1	38.9	1361.8	8.5
S_300 × 100 × 2-Gravel 20	300.1	99.9	2.0	49.4	36.1	38.9	615.2	2.0
S_180 × 60 × 3-Gravel 20	184.9	60.0	3.0	20.1	36.1	38.9	740.8	5.0

smoother steel surface, and the straining hardening effect may not be fully considered in existing design methods [17].

The combined use of stainless steel tubes and recycled aggregate concrete may offer both mechanical and environmental advantages, while the use of stainless steel could also help mitigate the drawbacks of recycled aggregates. This topic stems from research on concrete filled stainless steel tubular columns and has been studied in recent years. Through an experimental investigation involving 28 specimens, Yang and Ma [18] found that stainless steel composite columns with recycled aggregate concrete exhibit compressive and flexural behaviour similar to those with ordinary concrete, albeit with slight reductions in elastic modulus and bearing capacity. They also confirmed that the stainless steel enhances the performance of the infilled recycled aggregate concrete. Another experimental study by Tam et al. [19] suggested that replacing ordinary concrete with recycled aggregate concrete has a greater impact on the strength of stainless steel composite columns compared to carbon steel specimens, stainless steel provides advantages such as higher residual strength and reduced variation in compressive strength. Focusing on interfacial bond behaviour, Zhao et al. [20] concluded while the ultimate bond strength in stainless steel composite columns with recycled aggregate concrete is lower than that of conventional CFST sections, it can increase as the coarse recycled aggregates replacement ratio rises. After studying the axial and bond behaviour of stainless steel composite columns, Han et al. [21] concluded that these columns exhibit higher critical strain and more pronounced strengthening after peak load. However, the use of recycled aggregates reduces chemical adhesion due to greater shrinkage, and the smooth surface of stainless steel lowers interlocking forces. A recent study by Xu et al. [22] confirms that stainless steel composite columns demonstrate higher ductility and energy dissipation compared to conventional CFST columns, benefiting from stainless steel's strain hardening and cyclic hardening properties.

These recent studies have provided insights into the behaviour of stainless steel composite columns with recycled aggregate concrete

(a) Granite 10 mm (b) Recycled 10 mm

(c) Granite 20 mm (d) Gravel 20 mm

Fig. 1. Aggregates used in this research.

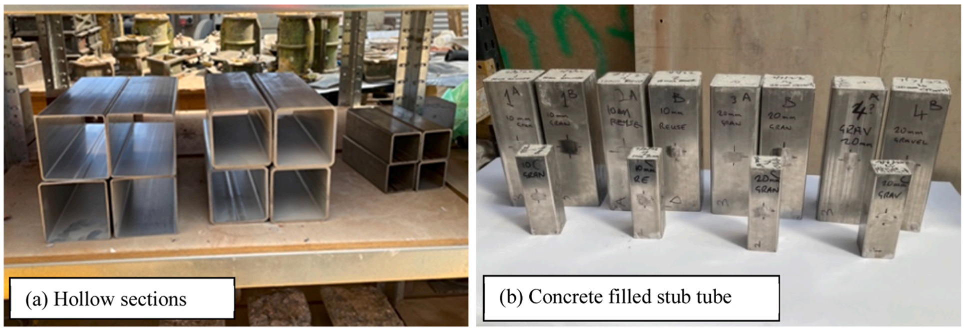

Fig. 2. Stainless steel hollow sections and concrete-filled stainless steel columns before testing.

under various conditions. They confirm that stainless steel composite columns with recycled aggregate concrete exhibit similar compressive and flexural behaviour to conventional CFST columns and higher ductility and energy dissipation capacity under lateral cyclic loading. Although the smooth surface of stainless steel reduces the bond performance at the steel-concrete interface, the introduction of recycled coarse aggregates can mitigate this effect, and the ultimate bond strength increases with the replacement ratio. However, it should be noted that these existing studies have primarily focused on the effects of the replacement ratio of recycled aggregates, whilst the effect of different types of recycled aggregates remains unexplored.

The research presented in this paper expands the experimental database on these columns, supporting the future development of design codes. An experimental programme was conducted to evaluate the compressive behaviour of stub composite column with duplex stainless steel square outer tubes and concrete made with different aggregates. The hypothesis is that the high performance of stainless steel can offset the disadvantages of recycled aggregates. Additional parametric studies and comparative analyses were performed to explore the effects of three common stainless steel types and two concrete strength classes on the axial compressive capacity of stub composite columns with various square cross sectional dimensions. Finally, a simple formula was proposed to predict the cross-sectional resistance under pure compression.

2. Experimental study

This section presents the experimental study and analyses the results.

2.1. Test specimens

The axial compressive behaviour and failure mode of concrete-filled stainless steel columns were investigated through an experiment involving 12 stub composite column specimens. The study examined the effects of cross-sectional dimensions, as well as the types and sizes of coarse aggregates, considering material availability and test facility constraints. Three types of stainless steel square sections were used, with sectional width by wall thickness of 100 mm × 5 mm, 100 mm × 2 mm, and 60 mm × 3 mm. All the stainless steel sections (lean duplex stainless steel EN 1.4162 [23]) were cold-formed and seam-welded. The measured dimensions are summarized in Table 1, where *L*, *B* and *t* denote the length, external width and wall thickness of the square hollow section. A limitation of the experiment was that absence of duplicate specimens; therefore, the test results should be interpreted with caution. Due to technical constraints, the mechanical properties were only available for the square stainless steel section with width of 60 mm by thickness of 3 mm. Coupons cut at flat region gave an elastic modulus of 209,800 MPa, a 0.2 % proof strength of 755 MPa, a 1.0 % proof strength of 819 MPa, an ultimate strength of 839 MPa, and a strain at fracture of 44 %. Coupons cut at corner region exhibited an elastic modulus of 212, 400 MPa, a 0.2 % proof strength of 885 MPa, a 1.0 % proof strength of 1024 MPa, an ultimate strength of 1026 MPa, and a strain at fracture of

Fig. 3. Test set-up for the specimens.

22 %.

The concrete was produced using four different types of coarse aggregates: 10 mm recycled aggregate, 10 mm crushed granite aggregate, 20 mm crushed granite aggregate and 20 mm uncrushed gravel aggregate. No tests were conducted on the mechanical properties of the coarse aggregates. The fine aggregate used was river sand. Ordinary Portland cement of 42.5 class was used. Fig. 1 shows the different aggregates used. The target compressive cube strength was designed to be 30 N/mm^2 at 28 days. The measured compressive cube strength of concrete at 28 days and test date are showed in Table 1. As shown, all four batches of concrete reached the target strength. The strength of concrete using 20 mm aggregates was about 20 % higher than the target strength. By comparison, although the recycled aggregate concrete reached the target strength of 30 N/mm^2, it had the lowest strength and exhibited a limited increase by the test date. The specimen *ID* in Table 1 represents the specimen's characteristics. For instance, "S_300 × 100 × 5-Granite 10" means the composite column has a length of 300 mm, an outer width of 100 mm, a wall thickness of 5 mm, using granite aggregate with a grain size of 10 mm. To achieve an even and uniform loading surface, high strength mortar was applied to both ends of the concrete-filled stub columns and allowed to harden before testing. Fig. 2 shows the stainless steel hollow sections and composite stub columns before testing.

2.2. Test set-up

All specimens were tested using an Avery Denison machine with a 2500 kN capacity, as shown in Fig. 3. A linear variable displacement transducer (LVDT) was used to measure the axial shortening of the specimens. Note that using a single LVDT could introduce errors, as the platens in the testing machine could cause slight uneven displacement or

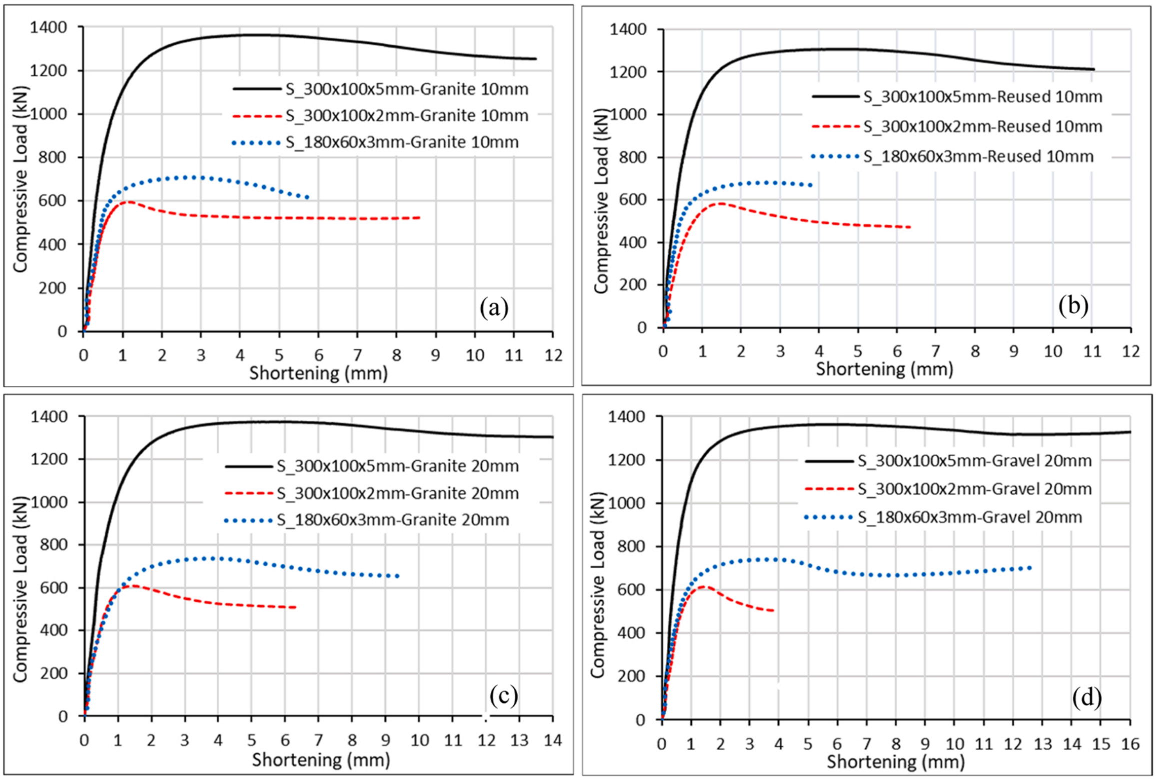

Fig. 4. Comparison of load-shortening curves showing the effect of different stainless steel hollow sections (a – Granite 10, b – Recycled 10, c – Granite 20, d – Gravel 20).

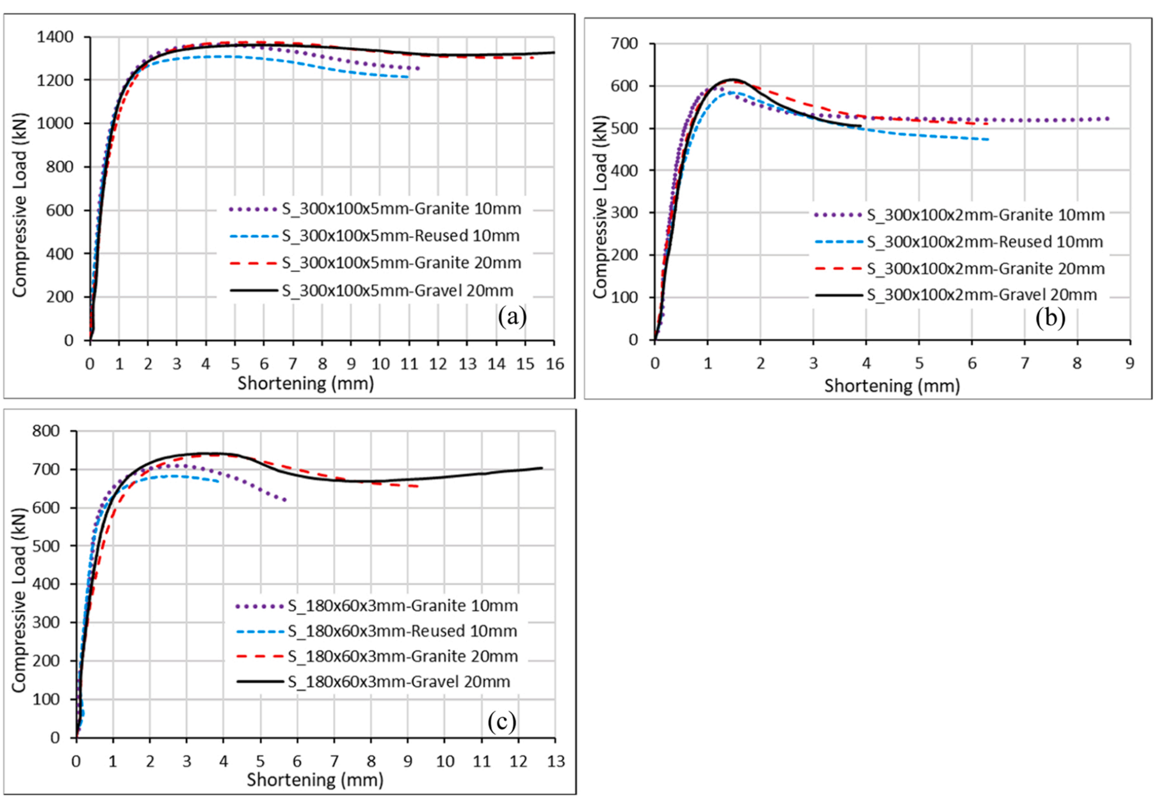

Fig. 5. Comparison of load-shortening curves showing the effect of different aggregates (a – S_300 ×100 ×5, b – S_300 ×100 ×2, c – S_180 ×60 ×5).

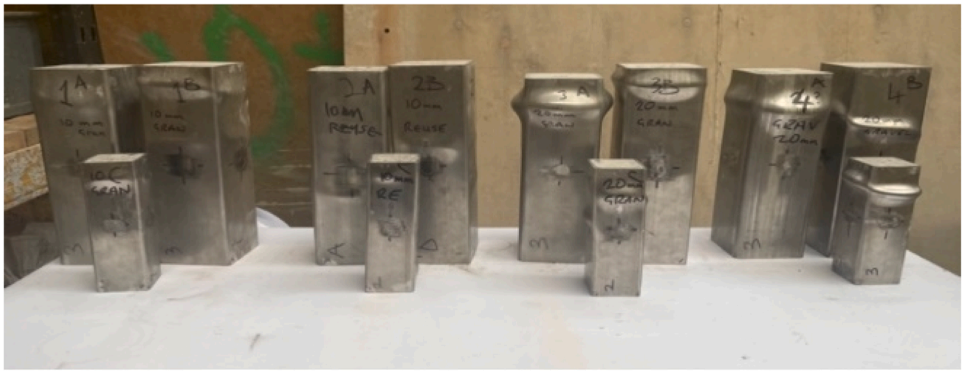

Fig. 6. Failure modes of specimens after testing (Aggregates from left to right: Granite 10, Recycled 10, Granite 20 and Gravel 20).

eccentricity. Four strain gauges were adhered to the external faces at the mid-height of each stainless steel section to measure strain. Two of the gauges measured longitudinal strain, while the other two detected hoop strain. Before loading, pre-compression was applied to remove the initial gap between the specimen and the loading plate and support plate. The loading rate was set at 0.45kN/s until either failure occurred or the test machine terminated automatically.

2.3. Axial compressive behaviour

This sub-section presents the results of axial behaviour, highlighting the effects of parameters. Fig. 4 compares the relationships of compressive load vs axial shortening, showing the effect of different stainless steel hollow sections. Specimens with the same type of coarse aggregate are grouped in one sub-figure. Obviously, the load capacity is dominated by the overall cross-sectional dimensions and the wall thickness of the stainless steel sections. Specimens with cross-sectional dimensions of 300 × 100 × 5 mm demonstrated the highest load capacity, followed by those with dimensions of 180 × 60 × 3 mm. Although the specimens with dimensions of 300 × 100 × 2 mm have a slightly larger cross-sectional area in the stainless steel tube compared to those with dimensions of 180 × 60 × 3 mm, their maximum load capacity is lower. This is likely due to the greater slenderness of the tube wall in the former. This greater slenderness resulted in early local buckling and a reduced confinement provided by the hollow section to concrete core.

Fig. 5 compares the compressive load vs shortening curves showing the effect of different aggregates. It can be seen the maximum loads of

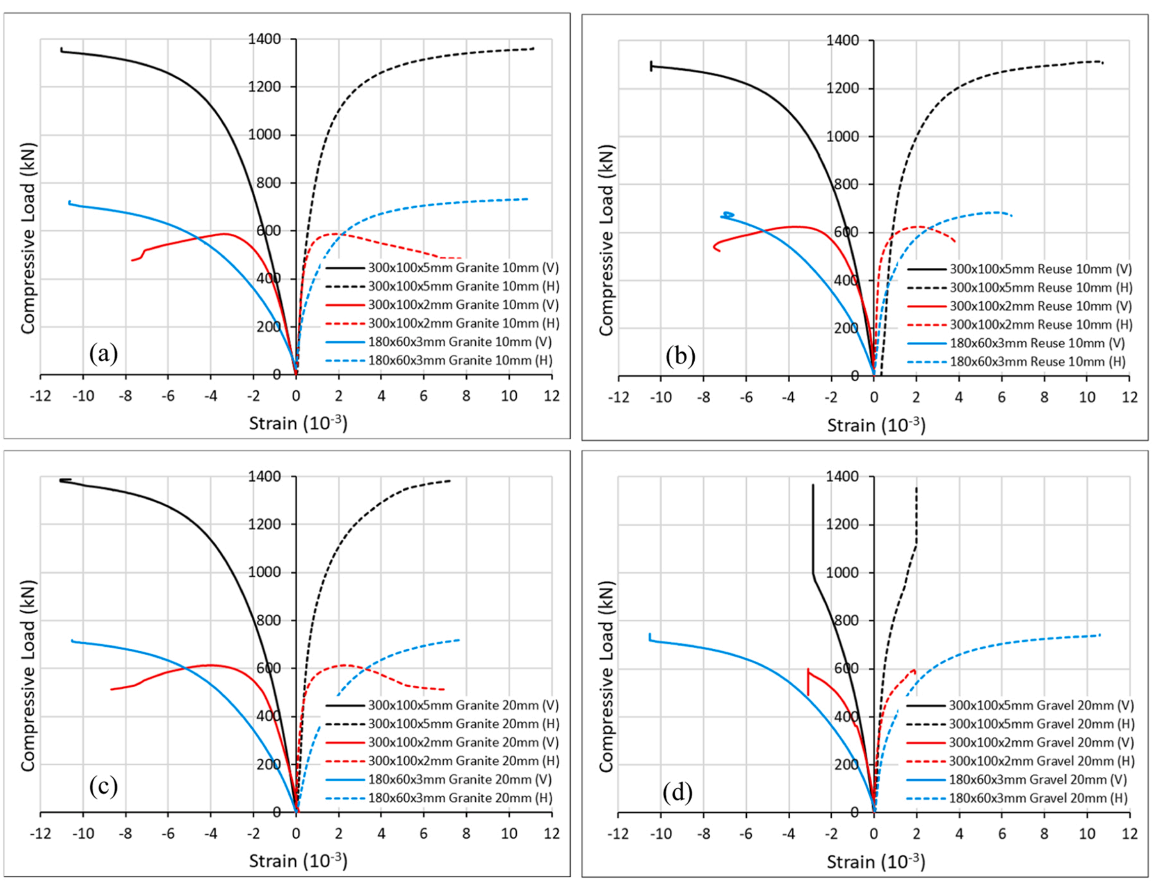

Fig. 7. Comparison of load-strain curves showing the effect of different stainless steel hollow sections (V: compressive strain, H: hoop strain, a – Granite 10, b – Recycled 10, c – Granite 20, d – Gravel 20).

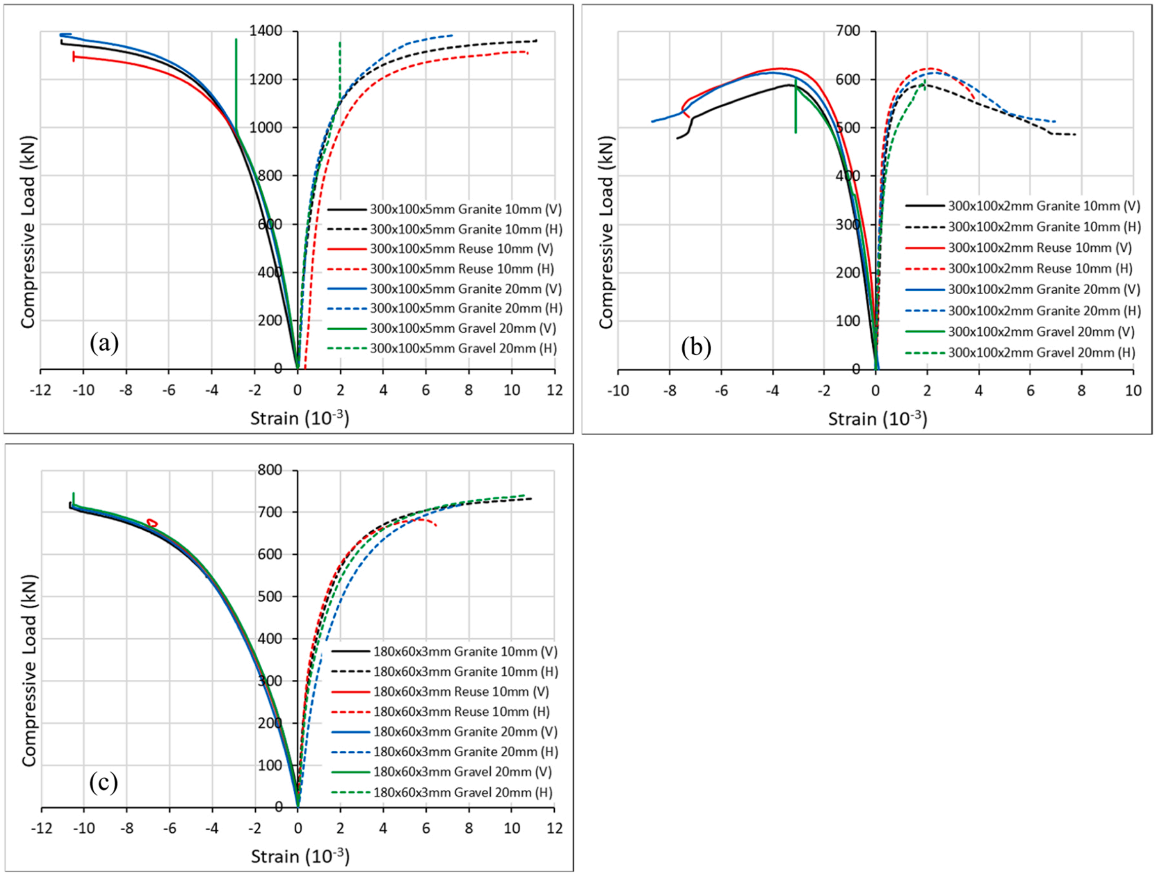

Fig. 8. Comparison of load-strain curves showing the effect of different aggregate concretes (V: compressive strain, H: hoop strain, a – S_300 ×100 ×5, b – S_300 ×100 ×2, c – S_180 ×60 ×5).

composite columns using 20mm-granite aggregate concrete and 20mm-gravel aggregate concrete are very similar and are the highest among the four batches. This is followed by the composite columns filled with concretes using 10mm-granite aggregates. Unsurprisingly, the load capacity of composite columns using recycled aggregates is the lowest. With the steel sections remained the same, the variation in load capacity is likely attributable to the differences in the strength of concrete at test date. As shown in Table 1, the concrete using 20 mm granite and 20mm-gravel aggregates attained the highest strengths, 38.2 MPa and 38.9 MPa respectively. The concrete using 10 mm granite aggregate has a strength of 33.0 MPa, which is 10 % higher than the strength of concrete using recycled aggregate 30.1 MPa. The variations in load capacity of composite stub columns clearly align with the strength of the infilled concrete.

2.4. Failure modes

Fig. 6 shows the failure modes of the composite specimens after testing. The failure modes were characterised by a local buckling mechanism. Bulges appeared on the surface, either near one end or at mid-height, protruding outwards. Inward bulging was restrained by the concrete core. These failure modes align with previous observations [18,19,21] and are consistent with expectations for stub columns.

2.5. Strain development

Fig. 7 compares the relationships between compressive load and axial strain (V) as well as hoop strain (H). The strain data was obtained from strain gauges arranged at the mid-height of the specimens, with the curves representing the average values from two strain gauges. The maximum recorded strain just exceeded 11,000 με; however, this should not be interpreted as the maximum strain in the steel tube, but rather as the strain measured at specific points. It is likely that the actual maximum strain in the stainless steel was not captured, as local buckling may have initiated elsewhere in the specimen, significantly influencing the failure of the short column.

For specimens using the same type of coarse aggregate, an increase in tube wall thickness appears to correspond with a higher measured strain at failure. However, for the specimen with 20 mm gravel aggregates, strain gauge issues prevented the recording of real strains at maximum load for tubes with dimensions of 300 × 100 × 5 mm and 300 × 100 × 2 mm (Fig. 7d). In general, specimens with cross-sectional dimensions of 300 × 100 × 5 mm and 180 × 60 × 3 mm exhibited higher strain capacity compared to those with 300 × 100 × 2 mm dimensions. This is likely due to the greater slenderness of the latter, which resulted in early local buckling, preventing the full development of strain capacity.

Fig. 8 compares the relationships between compressive load and axial strain (V) as well as hoop strain (H). In this figure, strain data for specimens with the same cross-sectional dimensions are grouped together to highlight the effects of different aggregate types in the concrete. It can be observed that, for specimens with identical dimensions, the type of infilled concrete has a minimal impact on strain development.

2.6. Main findings from tests

- The experimental study revealed that the typical failure mode of concrete-filled stainless steel stub hollow sections is local outwards buckling of the tube wall. The axial load capacity of stainless steel

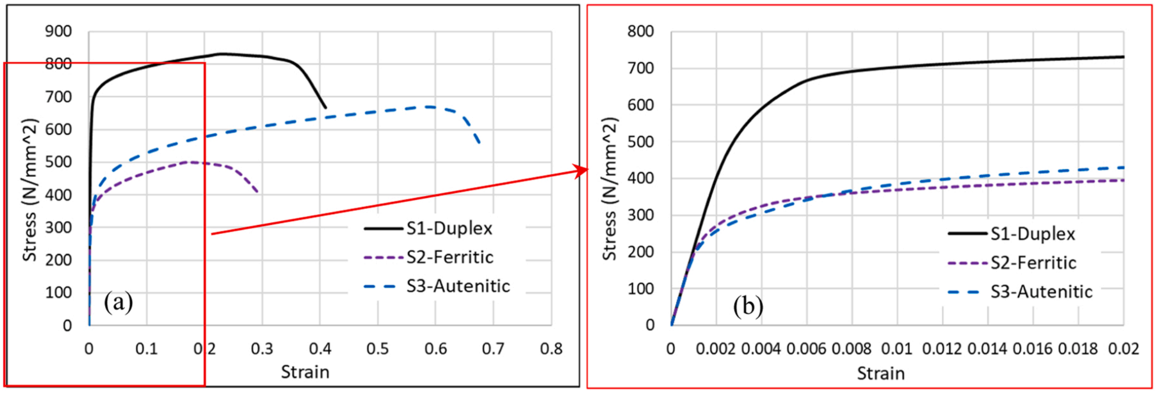

Fig. 9. Stress vs strain relationships of typical stainless steel for the parametric study (a – overall view, b – enlarged view).

composite stub column increases with the wall thickness. This is primarily due to the higher sectional compressive capacity of thicker steel tube, which also provides more effective confinement to the concrete core. This is further supported by the strain development, as it is observed that for the same type of coarse aggregate, an increase in tube wall thickness tends to correspond with a higher measured strain at failure.

- The load bearing capacity of the concrete-filled stainless steel stub column shows increasing trends as the strength of the infilled concrete increases. The type and size of the coarse aggregates affected compressive strength of concrete, however the change in load bearing capacity of the composite columns was not significant based on the limited tests conducted, and therefore, the experimental results should be interpreted with caution.

It is important to note that only one LVDT was used to obtain the displacement during the test, which could potentially introduce errors. Additionally, the lack of duplicate specimens means that result of each individual data point should be interpreted with caution.

3. Parametric study

3.1. Development of FE model

There is no doubt physical testing provides more realistic information about the behaviour of structural members. However, physical testing is both expensive and time-consuming, making it impractical for large-scale parametric studies. Consequently, numerical simulation has been extensively employed to explore the structural behaviour of concrete-filled steel tube columns. In this parametric study, a numerical simulation approach is adopted, using a finite element model (FEM) developed in ABAQUS/Standard [24]. The details of model development and validation have been reported in [15] and are summarised here. An elastic-plastic model was used for the stainless steel, while the Drucker–Prager model was used for the concrete core. A reference point was defined to couple together the top face of upper endplate, and load was applied via this reference point. A second reference point was defined to couple together the bottom face of the lower endplate and was used to apply boundary conditions. Only vertical displacement was allowed at the top end, while all other degrees of freedom were constrained to zero.

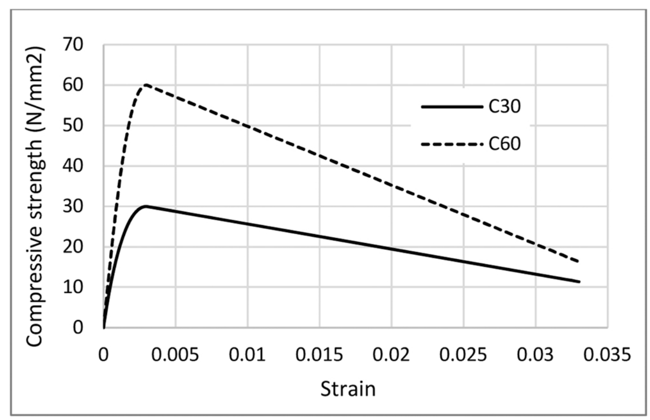

Fig. 10. Stress-strain relationships of concrete used in the parametric study.

Three-dimensional 8-node solid elements were used to simulate both the stainless steel tube and concrete core. The mesh size for the stainless steel was set equal to the wall thickness, whilst for the concrete core, the minimum mesh size was approximately twice the wall thickness. A minimum of two layers of meshes were applied to the stainless tube in the thickness direction.

3.2. Introduction of parameters

This parametric study was set out to investigate the effects of the type of the stainless steel, strength of infilled concrete and the cross-sectional dimensions on the structural behaviour. The parametric study presented covers three typical stainless steel families representing Austenitic stainless steel (Au), Ferritic stainless steel (Fe) and Duplex stainless steel (Du), two different concrete strengths (C30/37 and C60/75) and various cross-sectional dimensions ranging from the smallest 60 × 60 mm to largest 200 × 200 mm with wall thickness in the range from 2 mm to 10 mm. To avoid a global failure mechanism, the length of the composite columns is set to be 3 times of the maximum section width. A total of more than 150 column specimens were modelled to explore the effects of the component materials and cross-sectional dimensions on

Table 2
Summary of key mechanical properties of three types of stainless steel.

Stainless steel type	$\sigma_{0.1}$ (MPa)	$\sigma_{0.2}$ (MPa)	$\sigma_{1.0}$ (MPa)	σ_u (MPa)	$\varepsilon_{0.2}$	ε_u	ε_f	E (N/mm^2)
Austenitic (Au)	280	295	390	670	0.00341	0.56	0.68	210,000
Ferritic (Fe)	300	315	370	500	0.00350	0.16	0.30	210,000
Duplex (Du)	590	635	705	830	0.00502	0.22	0.41	210,000

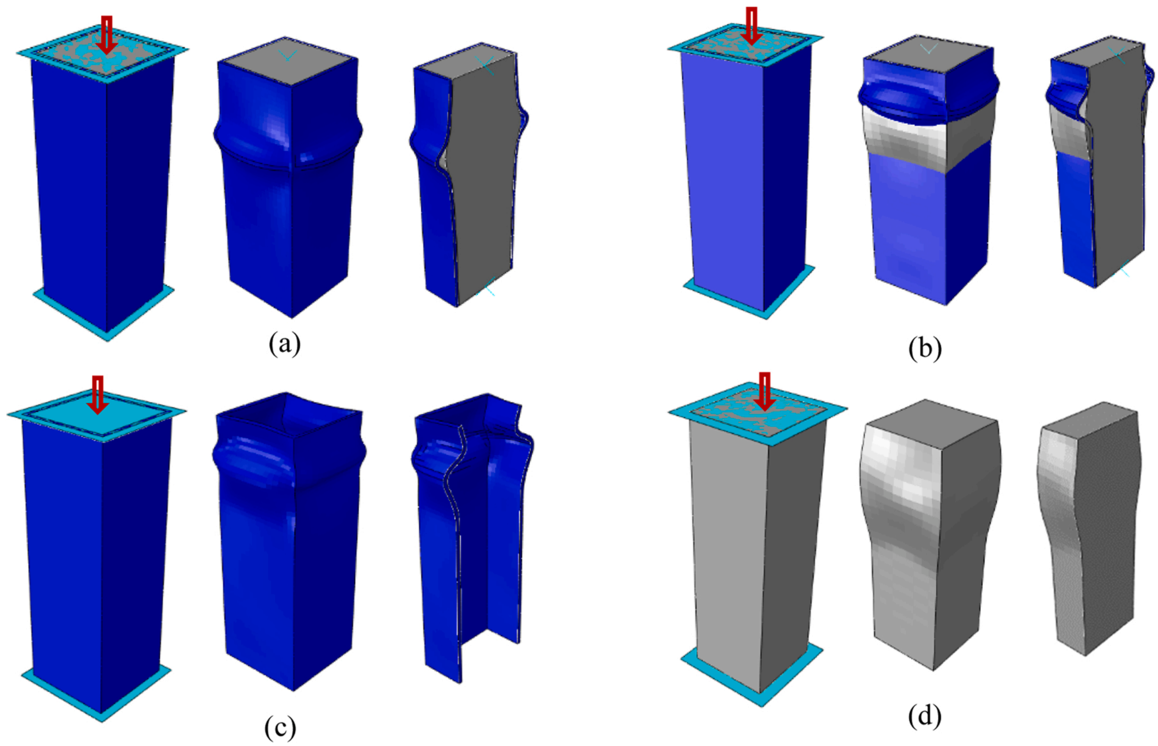

Fig. 11. Failure modes under different loading scenarios. (a. composite column with action between steel section and concrete core, b. composite column without action between steel section and concrete core, c. steel section only, and d, concrete core only).

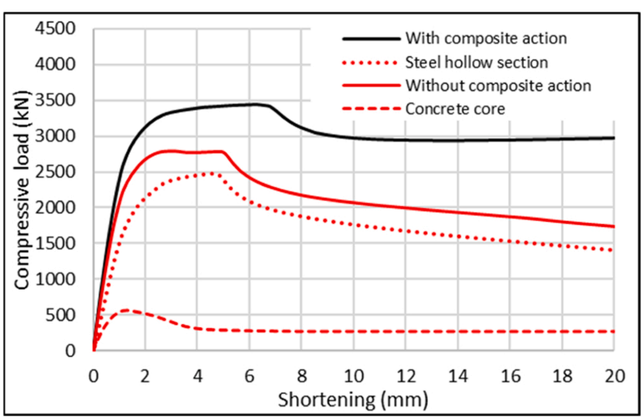

Fig. 12. Comparison of load vs shortening behaviour of stub composite column (450 ×150 ×6 mm, Duplex steel, C30 concrete) and constitutive component under compression.

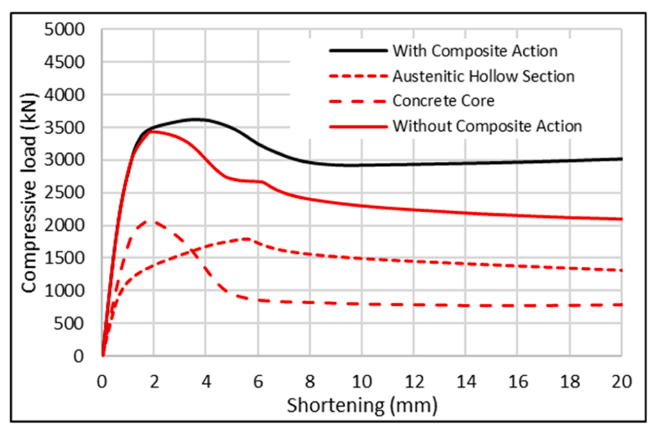

Fig. 13. Comparison of load vs shortening behaviour of composite column (600 ×200 ×6 mm, Austenitic steel, Concrete C60) and constitutive component under compression.

the axial compressive strength of concrete-filled stainless steel columns and the composite action mechanism. Fig. 9 shows the stress-strain curves adopted in the parametric study. These curves were generated based on the information and approach provided in [11] and represent three typical stainless steel families. Table 2 summarises the key data of the curves. Fig. 10 shows the stress-strain curves of unconfined concrete with compressive cylinder strengths, 30 N/mm^2 and 60 N/mm^2, used in the parametric study. In the FE modelling, the properties of the confined concrete were generated using methods provided in [12,15].

3.3. Composite action between steel tube and concrete core

To understand the composite effect, four scenarios were adopted to obtain the load vs shortening behaviour of a typical composite column (450 ×150 ×6 mm, Duplex stainless steel and C30 concrete) and individual constituent members. As shown in Fig. 11, the scenarios include: (a) composite columns with composite action between the steel hollow section and the concrete core, (b) composite columns without the above action, (c) steel hollow tube only, and (d) concrete core only. The difference in the failure modes in Fig. 11 indicates that the concrete core provides support to the tube wall and the steel tube section provides confinement to the infilled concrete. Consequently, different scenarios exhibit different load vs shortening behaviours as shown in Fig. 12. The maximum load (2785.3 kN, at shortening 2.96 mm) of hollow section and concrete under compression together but without composite action (scenario b) is different from the sum (3035.7 kN) of maximum loads of individual hollow section (scenario c, 2473.9 kN, at shortening 4.66 mm) and individual concrete core (scenario d, 561.8 kN, at shortening 1.18 mm) under axial compression. Both maximum loads are lower than the maximum load (scenario a, 3443.5 kN, at shortening

Table 3
Summary of specimen parameters and maximum axial compressive loads.

$L \times B \times t$ (mm)	B/t	Steel ID	N_0 (kN)	$N_{1,C30}$ (kN)	$N_{1,C60}$ (kN)	$N_{2,C30}$ (kN)	$N_{3,C30}$ (kN)	$N_{2,C60}$ (kN)	$N_{3,C60}$ (kN)
180 × 60 × 2	30	Du	335.4	93.6	187.3	424.7	409.8	493.8	475.4
	30	Fe	199.3			288.2	270.1	341.7	333.0
	30	Au	217.7			307.5	289.6	360.8	327.6
180 × 60 × 4	15	Du	714.2	80.6	161.4	1070.7	771.7	1070.6	808.8
	15	Fe	419.4			688.8	484.4	703.1	517.9
	15	Au	469.4			736.5	533.5	764.1	571.1
300 × 100 × 2	50	Du	406.4	273.5	548.8	741.0	679.3	1019.0	953.7
	50	Fe	263.3			535.3	520.5	796.9	788.8
	50	Au	262.7			536.6	508.8	782.5	775.3
300 × 100 × 4	25	Du	1099.7	251.9	503.5	1547.3	1258.7	1740.5	1434.5
	25	Fe	602.4			934.0	757.8	1120.9	981.7
	25	Au	654.0			1010.1	796.5	1179.4	954.3
300 × 100 × 6	16.7	Du	1738.1	230.4	460.7	2531.5	1859.5	2560.5	1940.1
	16.7	Fe	987.8			1604.6	1112.1	1664.2	1185.2
	16.7	Au	1104.8			1721.2	1239.4	1742.5	1307.9
450 × 150 × 2	75	Du	611.7	632.4	1267.3	1318.4	1235.6	1937.9	1872.3
	75	Fe	423.5			1013.9	997.6	1636.9	1629.7
	75	Au	430.2			998.4	976.1	1618.0	1608.3
450 × 150 × 4	37.5	Du	1421.2	595.1	1198.6	2156.8	1973.2	2711.0	2532.9
	37.5	Fe	835.8			1410.8	1339.3	1958.8	1913.8
	37.5	Au	834.8			1456.3	1306.7	1933.8	1873.4
450 × 150 × 6	25	Du	2473.9	561.8	1131.5	3443.5	2785.3	3873.4	3186.5
	25	Fe	1358.6			2080.2	1691.7	2522.7	2202.5
	25	Au	1471.4			2231.1	1760.7	2576.8	2139.3
450 × 150 × 8	18.8	Du	3407.7	529.4	1066.4	4947.5	3682.9	5159.9	3852.6
	18.8	Fe	1897.0			3052.8	2188.2	3354.5	2494.3
	18.8	Au	2111.2			3292.9	2398.8	3558.1	2549.9
600 × 200 × 2	100	Du	935.2	1126.2	2264.5	2107.1	2018.1	3178.9	3113.9
	100	Fe	622.1			1643.2	1610.9	2775.9	2749.0
	100	Au	659.1			1612.8	1583.5	2747.3	2721.7
600 × 200 × 4	50	Du	1714.0	1079.9	2171.6	2975.6	2774.1	4063.4	3853.0
	50	Fe	1076.7			2136.2	2069.1	3173.4	3137.9
	50	Au	1049.4			2139.8	2013.1	3128.8	3082.1
600 × 200 × 6	33.3	Du	3118.5	1034.8	2080.8	4267.6	3974.7	5163.2	4793.4
	33.3	Fe	1686.9			2701.8	2534.5	3621.3	3522.2
	33.3	Au	1782.5			2814.4	2468.7	3610.9	3439.3
600 × 200 × 8	25	Du	4404.9	990.4	1991.8	6120.1	4956.1	6884.8	5658.9
	25	Fe	2401			3686.5	2996.5	4472.6	3905.5
	25	Au	2621			3929.4	3134.4	4545.5	3793.9
600 × 200 × 10	20	Du	5634.2	947.1	1904.8	8145.5	6126.7	8671.5	6544.6
	20	Fe	3143.4			4937.7	3626.9	6088.2	4293.8
	20	Au	3482.8			5347.6	3973.9	5684.0	4214.6

6.33 mm) of composite column with composite action.

Fig. 13 shows the comparison of load vs shortening behaviour for another typical stub composite column (600 ×200 ×6 mm, Austenitic stainless steel, Concrete C60) and constituent individual components under axial compression, evidently the shortenings corresponding to maximum loads are different due to their composite features and different material properties, in which the maximum load of steel tube is 1783 kN corresponding to shortening 5.61 mm, the maximum load of concrete core is 2081 at shortening 1.77 mm. For composite column with or without composite action considered, the maximum loads are 3611 kN and 3439 kN at shortening 3.69 mm and 1.92 mm respectively. The sum of maximum loads of steel hollow section and concrete core (3864 kN) is greater than composite column with or without action considered. This is different from the previous example, in which the sum of maximum loads of steel hollow section and concrete core is lower than composite column with interaction considered. This is possibly due

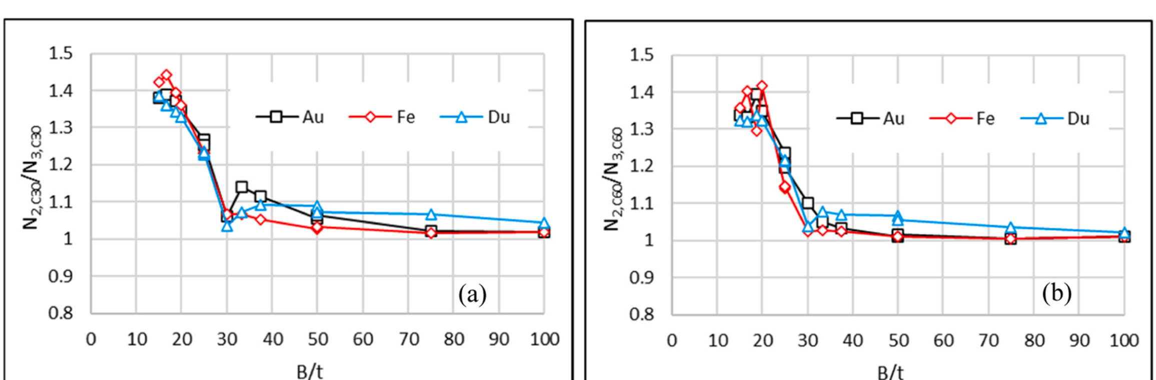

Fig. 14. Ratio of maximum load of composite columns with composite action to that in identical columns without composite action (a – C30, b – C60).

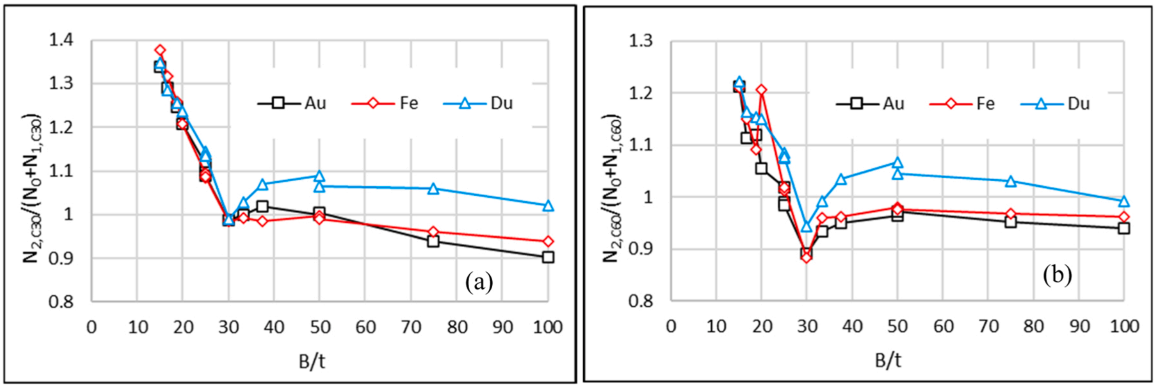

Fig. 15. Ratio of maximum load of composite columns with composite action to the sum of maximum loads in the hollow steel section and the concrete core (a – C30, b – C60).

to the smaller width/thickness ratio of hollow section provides higher confinement to the concrete core, thus higher enhancement of compressive capacity of stub composite column. The comparison of two cases suggests that, in design, the compressive capacity of a composite column section cannot be simply taken as the sum of maximum load capacities of the individual hollow section and concrete core. This simple addition may either overestimate or underestimate the actual load capacity of the composite column section.

3.4. Maximum axial compressive capacity

Table 3 summarizes the maximum compressive loads of stub composite columns with and without considering composite action and maximum compressive loads of individual constituent members. In which $L\times B\times t$ represents the column length, cross-sectional width, and wall thickness, N_0 is the maximum axial compressive load of steel hollow section. $N_{1,C30}$ and $N_{1,C60}$ are the maximum axial compressive loads of concrete core using C30 and C60 concrete respectively. $N_{2,C30}$ and $N_{2,C60}$ are the maximum axial compressive loads of the composite columns with C30 and C60 concrete respectively, composite action between steel tube and concrete core considered (scenario a). $N_{3,C30}$ and $N_{3,C60}$ are the maximum axial compressive loads of the composite columns with C30 and C60 concrete respectively, but the composite action between steel hollow section and concrete core is ignored (scenario b). Although the steel section and concrete core have the same axial shortening in scenario b, the steel tube does not provide confinement to concrete core, concrete core does not mitigate the inwards local buckling mechanism of tube wall.

3.5. Effects of steel type, concrete strength, $\boldsymbol{B/t}$ ratio and sectional dimensions

Fig. 14 compares the ratios of maximum load of composite columns with composite action ($N_{2,C30}$, $N_{2,C60}$) to that of identical composite columns without composite action ($N_{3,C30}$, $N_{3,C60}$). It can be seen that as B/t increases, the ratio of $N_{2,C30}/N_{3,C30}$, or $N_{2,C60}/N_{3,C60}$ decreases. This is mainly because the steel tube with lower B/t value provides higher confinement to the concrete core. However, when the B/t ratio is over than 30, the composite action reduced and increment of maximum compressive load is mostly less than 10 %, i.e., the ratios between 1.0 and 1.1. The lower the B/t value, the higher the ratios of $N_{2,C30}/N_{3,C30}$ and $N_{2,C60}/N_{3,C60}$. The highest ratio over 1.4 is attained when the B/t value is about 15. For different stainless steel types, the ratio vs B/t curves are slightly different attributed to the different mechanical properties of stainless steel. Nevertheless, the trends in change are very similar although the duplex stainless steel provides a stronger increase owing to its higher material strength. Comparing the ratios of composite columns with different concrete strengths, it appears the composite column with lower concrete strength shows a slightly higher maximum load increase. This indicates the confinement is more pronounced for concrete core with lower strength.

Fig. 15 compares the ratios of maximum load of composite columns with composite action ($N_{2,C30}$, $N_{2,C60}$) to the sum of maximum loads in the hollow steel tube (N_0) and the concrete core ($N_{1,C30}$, $N_{1,C60}$). It can be seen that when B/t increases, the ratios of $N_{2,C30}/(N_0+N_{1,C30})$ vs B/t and $N_{2,C60}/(N_0+N_{1,C60})$ vs B/t show similar trends, however when the B/t value is over than 30, the ratios of $N_{2,C30}/(N_0+N_{1,C30})$ and $N_{2,C60}/(N_0+N_{1,C60})$ may be lower than 1.0 for composite columns with Austenitic and Ferritic stainless steels. Note that this does not necessarily

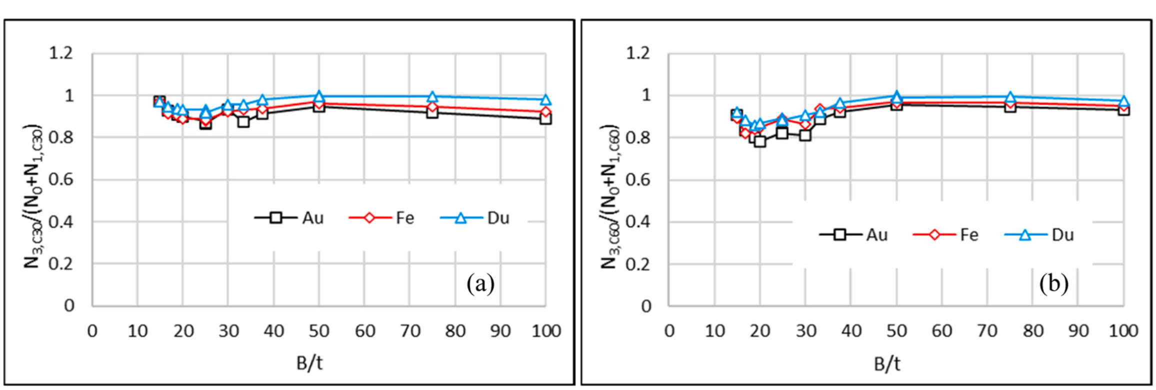

Fig. 16. Ratio of maximum load of columns without composite action to the sum of maximum loads in the individual hollow steel tube and concrete core (a – C30, b – C60).

Table 4
Summary of maximum compressive loads obtained from experiments and predicted by Eq.2.

Specimen ID	B/t	N_{t-max} (kN)	f_{cu} (N/mm^2)	N_{EC4} (kN) (Eq.2)	N_{t-max}/N_{EC4}
S_300 × 100 × 5-Granite 10	19.97	1362.8	33.0	1379.92	0.988
S_300 × 100 × 2-Granite 10	49.50	594.9	33.0	568.25	1.047
S_180 × 60 × 3-Granite 10	19.66	709.1	33.0	658.30	1.077
S_300 × 100 × 5-Reused 10	20.09	1308.5	30.0	1360.06	0.962
S_300 × 100 × 2-Reused 10	49.93	583.4	30.0	551.39	1.058
S_180 × 60 × 3-Reused 10	19.75	682.1	30.0	652.05	1.046
S_300 × 100 × 5-Granite 20	19.69	1374.7	38.2	1434.80	0.958
S_300 × 100 × 2-Granite 20	49.53	611.2	38.2	611.80	0.999
S_180 × 60 × 3-Granite 20	20.01	737.8	38.2	664.82	1.110
S_300 × 100 × 5-Gravel 20	19.92	1361.8	38.9	1424.72	0.956
S_300 × 100 × 2-Gravel 20	49.44	615.2	38.9	613.90	1.002
S_180 × 60 × 3-Gravel 20	20.13	740.8	38.9	661.76	1.119
Average					1.027
Standard Deviation					0.058

mean these composite columns exhibit no composite action between the steel section and the concrete core. Instead, this is mainly because the maximum loads of individual concrete core and individual hollow section occurred at different shortening due to the two materials have different stress-stain properties. This indicates that, for composite columns using Austenitic and Ferritic stainless steels with B/t values over 30, if the sum of maximum loads of individual tube and individual concrete core is used to estimate the maximum load capacity of the composite column, it might overestimate the axial compressive capacity of composite columns.

Fig. 16 compares the ratio of maximum load of columns without composite action ($N_{3,C30}$, $N_{3,C60}$) to the sum of maximum loads of the individual hollow steel tube (N_0) and individual concrete core ($N_{1,C30}$, $N_{1,C60}$), it can be seen the ratios of $N_{3,C30}/(N_0+N_{1,C30})$ and $N_{3,C60}/(N_0+N_{1,C60})$ are less than 1.0. This because the steel hollow section and concrete core reach the maximum axial loads at different shortenings (strain) due to different material mechanical behaviour, as shown in Fig. 12 and Fig. 13.

4. Prediction of axial compressive capacity

4.1. Design resistance by EC4

EC4 [25] provides a simple formula for the design resistance of carbon steel-concrete composite section under axial compression:

$$N_{EC4} = A_a f_{yd} + 0.85 A_c f_{cd} + A_s f_{sd} \quad (1)$$

Where, A_a is the cross-sectional area of structural steel, f_{yd} is the design value of the yield strength of structural steel, A_c is the cross-sectional area of concrete, f_{cd} is the design value of the compressive strength of concrete, A_s is the cross-sectional area of reinforcement, and f_{sd} is the design value of the yield strength of the reinforcing steel. For concrete-filled steel tubular section without reinforcement, Eq.1 may be simplified as Eq.2. To compare the axial compressive resistance of composite column provided by the Eurocode 4 with those obtained from experiments and numerical simulation in the parametric study, the factor 0.85 in the equation Eq.1 is replaced by 1.0 in Eq.2, the reinforcement contribution term is omitted.

$$N_{EC4} = N_s + N_c = A_a f_y + A_c f_c \quad (2)$$

Where, A_a is the cross-sectional area of stainless steel tube, f_y is the key characteristic strength of stainless steel, A_c, is the cross-sectional area of concrete core, and f_c is the cylinder compressive strength of concrete.

4.2. Comparison of maximum axial loads obtained from tests and predicted by Eq.2

The tested specimens were made from duplex stainless steel. In the prediction using Eq.2, the key characteristic strength of duplex stainless steel f_y was taken as the 0.2 % strain proof strength. Table 4 summarises the maximum loads and ratio of N_{t-max}/N_{EC4}. Results show that the average ratio of maximum test load to predicted resistance is 1.027 with a standard deviation of 0.058. Although the strength of concrete varies with different aggregates, it is difficult to identify a clear correlation between the ratio of N_{t-max}/N_{EC4} and the concrete strength. However, the cross-sectional dimension of steel tube and B/t value affected the ratio of N_{t-max}/N_{EC4}. The lower the B/t value may result in a higher the ratio. This may be attributed to the stronger confinement provided by the steel tube. It should be noted that the tested specimen might have minor imperfection but was not measured. The imperfection might reduce the composite column axial compressive capacity.

4.3. Comparison of maximum axial loads obtained from parametric study to those predicted by Eq.2

As shown in the parameter study sections, the selected characteristic mechanical properties of three typical stainless steels are shown in

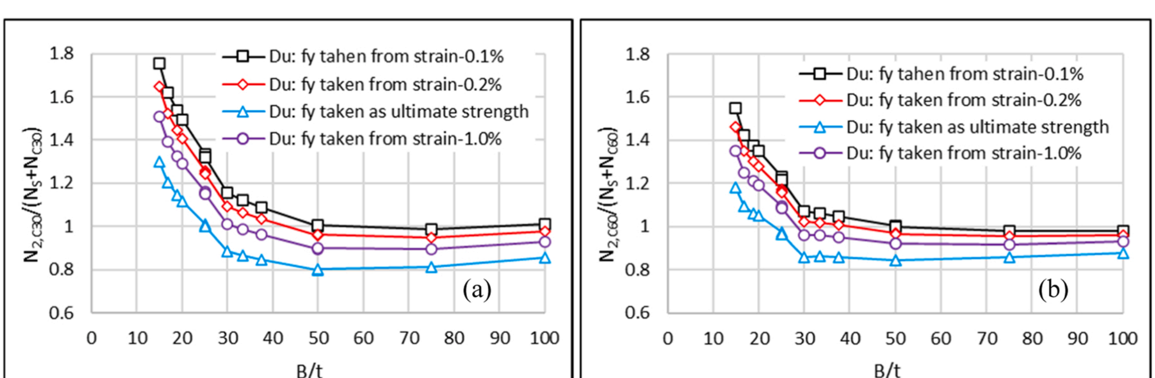

Fig. 17. Ratios of maximum load of composite columns with composite action to the predicted results by Eq.2 for duplex stainless steel (a – C30, b – C60).

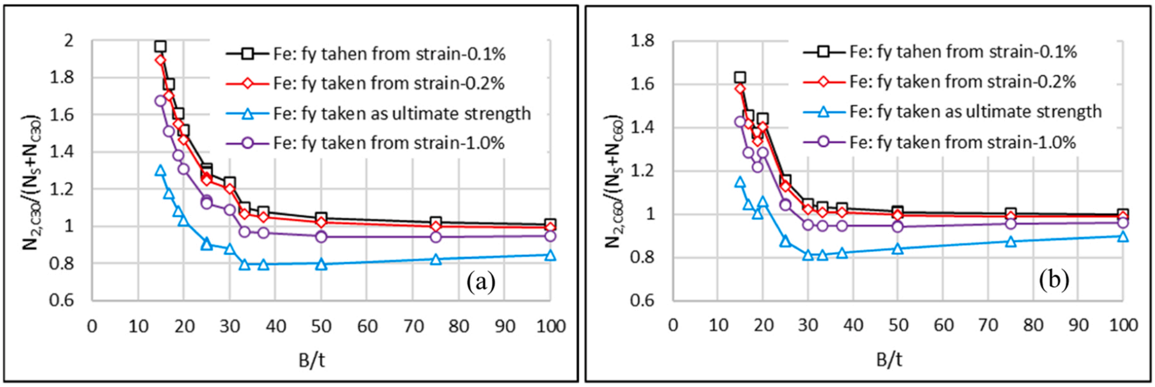

Fig. 18. Ratios of maximum load of composite columns with composite action to the predicted results by Eq.2 for ferritic stainless steel (a – C30, b – C60).

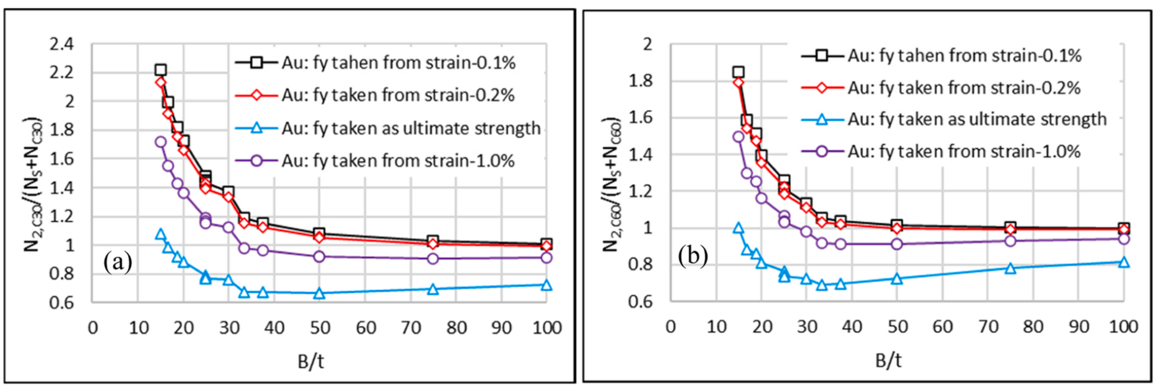

Fig. 19. Ratios of maximum load of composite columns with composite action to the predicted results by Eq.2 for austenitic stainless steel (a – C30, b – C60).

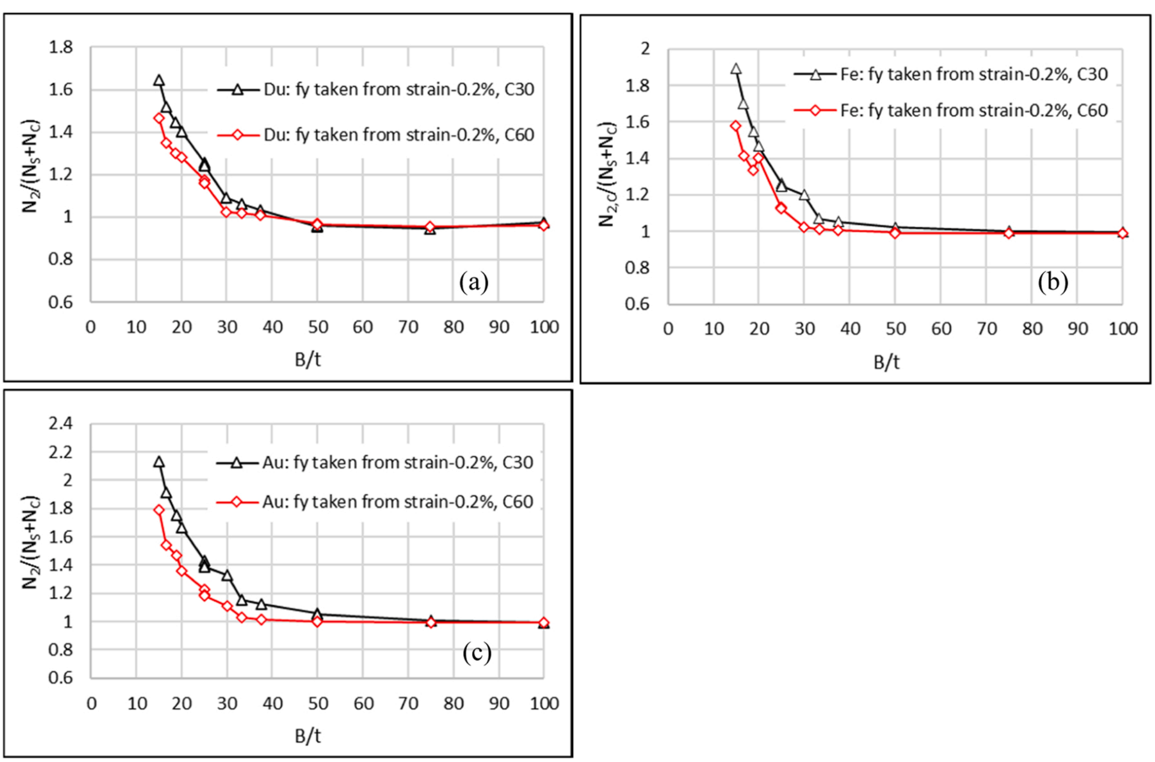

Fig. 20. Comparison of effect of concrete strength on maximum load ratio (a – Duplex, b – Ferritic, c - Austenitic).

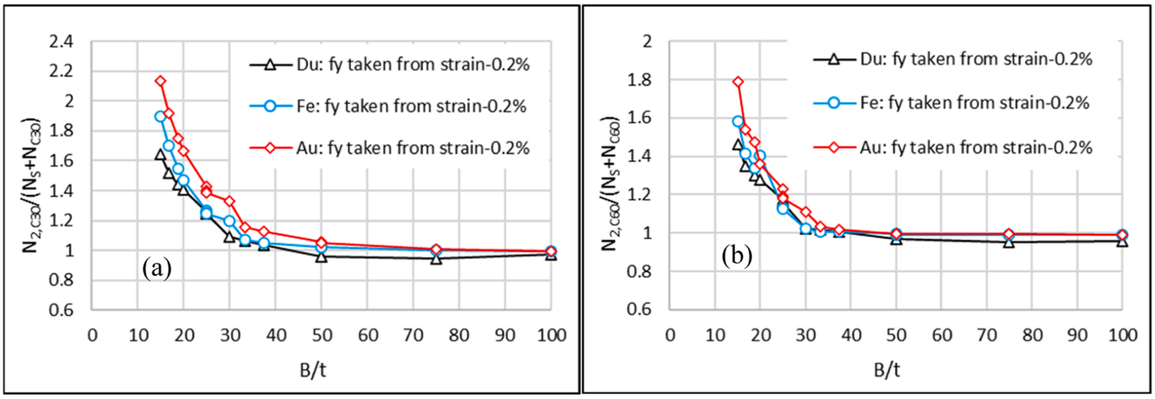

Fig. 21. Comparison of effect of stainless steel type on maximum load ratio (a – C30, b – C60).

Table 2, therefore in the prediction using Eq.2, different key characteristic strength of stainless steel, i.e. 0.1 % strain proof strength, 0.2 % strain proof strength, 1.0 % strain proof strength and ultimate strength were taken as f_y, to calculate the axial compressive resistance and then calculate the ratio of maximum load obtained from parametric study to the axial compressive resistance predicted by Eq.2. Two cylinder strengths of concrete, 30 N/mm^2 and 60 N/mm^2, were used in the parametric study and Eq.2 prediction.

Fig. 17, Fig. 18 and Fig. 19 compare the ratios of maximum compressive loads obtained from numerical simulation to the axial compressive resistance predicted using Eq.2. It can be seen for composite columns with lower B/t, the ratios are higher. For composite columns with higher B/t values, the ratios are close to 1.0. The ratio vs B/t relationships are significantly affected by the f_y values adopted. Providing the numerical modelling gives the true maximum axial loads, the comparison might indicate that Eq.2 may underestimate the axial compressive capacities of the composite columns when the B/t ratio is lower, although this is less noticeable for composite columns with higher B/t values, i.e. lesser confinement effect to concrete core from stainless steel hollow section. Regarding the effect of f_y value, using 0.2 % strain proof strength gives better results although using 0.1 strain proof strength gives very close curve trend. Using 1.0 % strain proof strength and ultimate strength overestimated the axial compressive capacity of composite columns. The promotion of axial compressive resistance of composite columns using lower concrete strength appears stronger than that of composite columns using higher concrete strength as shown in Fig. 20. This may be attributed to the stronger and more effective confinement effect for concrete with a lower strength. Although different stainless steel types have been used, the trends of load ratios vs B/t curves are similar. Nevertheless, some differences may be found as shown in Fig. 21.

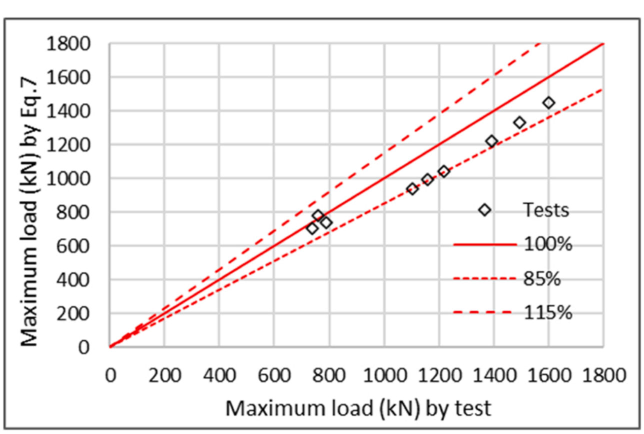

Fig. 22. Comparison of maximum loads obtained from tests [15] and Eq.7 predictions.

The above comparison and analysis indicate that Eq.2 cannot satisfactorily predict the compressive capacity of composite column; it significantly underestimates the capacity of composite column when the B/t value is lower but slightly overestimates that of composite columns using duplex stainless steel with higher B/t.

5. Proposed method for prediction of axial compressive capacity

The previous sections showed that the experimental load capacity of composite columns has a clear relationship with the axial resistance predicted using Eq.2 and selected strain proof strength of stainless steel and concrete cylinder compressive strength. However, the prediction may overestimate or underestimate the compressive loads depending on the steel cross-sectional features, concrete strength, stainless steel type and characteristic steel strength adopted. To provide a better prediction for the axial compressive capacity of square concrete-filled stainless steel columns, a revised coefficient is adopted for Eq.2 and a new formula Eq.3 is proposed as follows,

$$N_{PR} = \phi\left(A_a f_y + A_c f_c\right) \tag{3}$$

where, A_a is the cross-sectional area of stainless steel tube, f_y is the 0.2 % strain proof strength, A_c, is the cross-sectional area of concrete core, f_c is the cylinder compressive strength of concrete, and ϕ is a factor to consider both the confinement of steel section to the concrete core and the support provided by the concrete core for the hollow section wall.

Using the regression approach to analyse results obtained from parametric study and load ratios presented in previous sections, the following formulas are developed for the ϕ factor for different types of stainless steel. Eqs.4, 5 and 6 are for duplex, ferritic and austenitic stainless steel respectively. Considering ϕ factors are similar for three stainless steel types, Eq.7 is proposed for all stainless steel for a quick estimation.

For Duplex stainless steel:

$$\phi = (0.0012 - 0.000006667 f_c) \bullet (B/t)^2 - (0.0965 - 0.00061 f_c) \bullet (B/t) + (2.9865 - 0.0136 f_c),\ \text{for } 15 < B/t \le 35$$

$$\phi = (0.00011 - 0.000001333 f_c) \bullet (B/t)^2 - (0.0151 - 0.00017 f_c) \bullet (B/t) + (1.4573 - 0.0052 f_c),\ \text{for} 35 < B/t < 100 \tag{4}$$

For Ferritic stainless steel:

$$\phi = (0.0024 - 0.00001667 f_c) \bullet (B/t)^2 - (0.1697 - 0.00119 f_c) \bullet (B/t) + (4.1258 - 0.0234 f_c),\ \text{for } 15 < B/t \le 35$$

$$\phi = (0.000031 - 0.0000003667 f_c) \bullet (B/t)^2 - (0.0062 - 0.00008 f_c) \bullet (B/t) + (1.2765 - 0.0038 f_c),\ \text{for} 35 < B/t < 100 \tag{5}$$

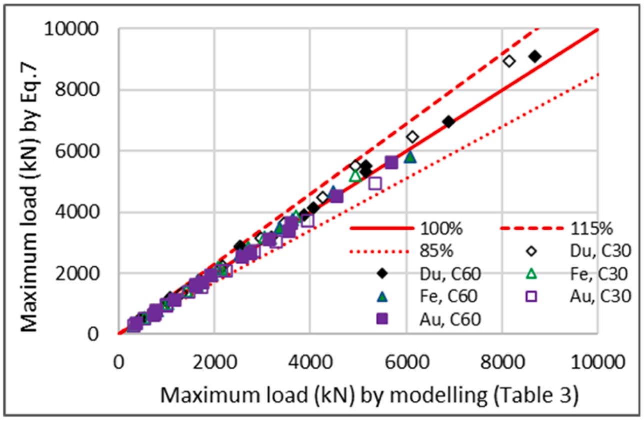

Fig. 23. Comparison of maximum loads obtained from modelling and Eq.7 predictions.

For Austenitic stainless steel:

$$\phi = (0.0022 - 0.000006667f_c) \bullet (B/t)^2 - (0.1674 - 0.00075f_c) \bullet (B/t) + (4.4565 - 0.0217f_c), \text{for} 15 < B/t \leq 35$$

$$\phi = (0.00009 - 0.000001333f_c) \bullet (B/t)^2 - (0.0152 - 0.00022f_c) \bullet (B/t) + (1.6707 - 0.0099f_c), \text{for} 35 < B/t < 100 \quad (6)$$

Average factor ϕ:

$$\phi = (0.001933 - 0.00001f_c) \bullet (B/t)^2 - (0.14453 - 0.00085f_c) \bullet (B/t) + (3.8563 - 0.01958f_c), \text{for} 15 < B/t \leq 35$$

$$\phi = (0.000077 - 0.0000010111f_c) \bullet (B/t)^2 - (0.01217 - 0.000154f_c) \bullet (B/t) + (1.4682 - 0.0063f_c), \text{for} 35 < B/t < 100 \quad (7)$$

In the above equations, B is the outer width of square tube, t is the thickness of tube wall, f_c is the cylinder compressive strength of core concrete. The coefficient ϕ is expected to cover the strength enhancement of concrete provided by steel hollow section confinement and mitigation of outwards local buckling provided by concrete core to tube wall. Fig. 22 shows a comparison of test results [15] with Eq.7 predictions, the maximum difference is less than 15 % with average Eq.7 prediction/test result ratio 0.91 and standard deviation 0.058. Fig. 23 compares the maximum axial loads ($N_{2,C30}$, $N_{2,C60}$) shown in Table 3 with the Eq.7 prediction for stub composite columns with three different stainless steels and two concrete strengths, good agreement achieved, the maximum difference is less than 15 % with average Eq.7 prediction/modelling result ratio 1.006 and standard deviation 0.054.

6. Conclusions

An experimental study, numerical modelling and analysis were conducted to evaluate the structural behaviour of stainless steel tubular stub columns infilled with concrete incorporating different coarse aggregates. The following conclusions may be drawn.

- The types and sizes of coarse aggregate influenced the compressive strength of concrete. However, based on the findings of this study, aggregate sizes of 10 mm and 20 mm did not significantly impact the axial compressive strength of concrete-filled stainless steel composite columns.
- The axial compressive capacity of concrete-filled stainless steel columns was significantly influenced by the type of stainless steel due to its distinct material properties.
- The axial compressive resistance is also significantly influenced by the cross-sectional width-to-wall thickness ratio, due to the composite action between the steel tube and concrete core. A lower cross-sectional width-to-wall thickness ratio results in greater confinement of the concrete core.
- Based on the Eurocode 4 prediction method, a new formula is proposed to predict the cross-sectional capacity of concrete-filled stainless steel composite columns subjected to axial compression. The comparison showed that the proposed formula could provide an acceptable prediction on the axial capacity of the concrete-filled stainless steel stub columns.

It should be noted that the above conclusions are based on a limited number of specimens in the experiment and are applicable only within the range of parameters considered in the parametric study. The properties of coarse aggregates, particularly the recycled coarse aggregates, may vary and even be subject to contamination, therefore, the effects of coarse aggregates should be interpreted with caution. Further research may be focused on the response of concrete-filled stainless steel columns under different conditions, such as high temperatures and dynamic loads. Additionally, a life cycle assessment of the combined use of stainless steel and recycled aggregate concrete could also provide valuable insights into its overall environmental impact.

CRediT authorship contribution statement

Yang Jie: Writing – review & editing, Writing – original draft, Methodology, Investigation, Formal analysis, Conceptualization. **Zhou Kan:** Writing – review & editing, Writing – original draft, Methodology, Investigation, Formal analysis, Conceptualization. **Dai Xianghe:** Writing – review & editing, Writing – original draft, Methodology, Investigation, Formal analysis, Conceptualization.

Declaration of Competing Interest

This paper has no conflict of interest with other people, organizations.

Acknowledgements

The authors would like to thank to Mr Stephen Robison and Mr Isiaka Tunde Alabi, in the University of Bradford, for their preparation for specimens and assistance in the experiments.

References

[1] Thai S, Thai H-T, Uy B, Ngo T. Concrete-filled steel tubular columns: test database, design and calibration. J Constr Steel Res 2019;157:161–81. https://doi.org/10.1016/j.jcsr.2019.02.024.

[2] Uy B, Tao Z, Han L-H. Behaviour of short and slender concrete-filled stainless steel tubular columns. J Constr Steel Res 2011;67(3):360–78. https://doi.org/10.1016/j.jcsr.2010.10.004.

[3] Wang B, Yan L, Fu Q, Kasal B. A comprehensive review on recycled aggregate and recycled aggregate concrete. Resour, Conserv Recycl 2021;171:105565. https://doi.org/10.1016/j.resconrec.2021.105565.

[4] Fu YYou, Lin Hai H, Xin W. Concrete shrinkage and creep in recycled aggregate concrete-filled steel tubes. Adv Struct Eng 2008;11(4):383–96. https://doi.org/10.1260/136943308785836772.

[5] Fathifazl G, Ghani Razaqpur A, Burkan Isgor O, Abbas A, Fournier B, Foo S. Creep and drying shrinkage characteristics of concrete produced with coarse recycled concrete aggregate. Cem Concr Compos 2011;33(10):1026–37. https://doi.org/10.1016/j.cemconcomp.2011.08.004.

[6] Debieb F, Kenai S. The use of coarse and fine crushed bricks as aggregate in concrete. Constr Build Mater 2008;22(5):886–93. https://doi.org/10.1016/j.conbuildmat.2006.12.013.

[7] Muhammad F, Harun M, Ahmed A, Kabir N, Khalid HR, Hanif A. Influence of bonded mortar on recycled aggregate concrete properties: a review. Constr Build Mater 2024;432:136564. https://doi.org/10.1016/j.conbuildmat.2024.136564.

[8] Chen J, Wang Y, Roeder CW, Ma J. Behavior of normal-strength recycled aggregate concrete filled steel tubes under combined loading. Eng Struct 2017;130:23–40. https://doi.org/10.1016/j.engstruct.2016.09.046.
[9] Wu L, Sun Z, Cao Y. Modification of recycled aggregate and conservation and application of recycled aggregate concrete: a review. Constr Build Mater 2024;431:136567. https://doi.org/10.1016/j.conbuildmat.2024.136567.
[10] Nikolić J, Tošić N, Murcia-Delso J, Kostić SM. Comprehensive review of the structural behaviour and numerical modelling of recycled aggregate concrete-filled steel tubes. Eng Struct 2024;303:117514. https://doi.org/10.1016/j.engstruct.2024.117514.
[11] Arrayago I, Real E, Gardner L. Description of stress–strain curves for stainless steel alloys. Mater Des 2015;87:540–52. https://doi.org/10.1016/j.matdes.2015.08.001.
[12] Ellobody E, Young B. Design and behaviour of concrete-filled cold-formed stainless steel tube columns. Eng Struct 2006;28(5):716–28. https://doi.org/10.1016/j.engstruct.2005.09.023.
[13] Lam D, Gardner L, Burdett M. Behaviour of Axially Loaded Concrete Filled Stainless Steel Elliptical Stub Columns. Adv Struct Eng 2010;13(3):493–500. https://doi.org/10.1260/1369-4332.13.3.493.
[14] Patel VI, Liang QQ, Hadi MNS. Nonlinear analysis of axially loaded circular concrete-filled stainless steel tubular short columns. J Constr Steel Res 2014;101:9–18. https://doi.org/10.1016/j.jcsr.2014.04.036.
[15] Lam D, Yang J, Dai X. Finite element analysis of concrete filled lean duplex stainless steel columns. Structures 2019;21:150–5. https://doi.org/10.1016/j.istruc.2019.01.024.
[16] Lai B-L, Zheng X-F, Fan S-G, Chang Z-Q. Behavior and design of concrete filled stainless steel tubular columns under concentric and eccentric compressive loading. J Constr Steel Res 2024;213:108319. https://doi.org/10.1016/j.jcsr.2023.108319.
[17] Han L-H, Xu C-Y, Tao Z. Performance of concrete filled stainless steel tubular (CFSST) columns and joints: summary of recent research. J Constr Steel Res 2019;152:117–31. https://doi.org/10.1016/j.jcsr.2018.02.038.
[18] Yang Y-F, Ma G-L. Experimental behaviour of recycled aggregate concrete filled stainless steel tube stub columns and beams. Thin Walled Struct 2013;66:62–75. https://doi.org/10.1016/j.tws.2013.01.017.
[19] Tam VWY, Wang Z-B, Tao Z. Behaviour of recycled aggregate concrete filled stainless steel stub columns. Mater Struct 2014;47(1):293–310. https://doi.org/10.1617/s11527-013-0061-1.
[20] Zhao H, Li J, Wang R, Lam D, Zhang Y. Study on interfacial bond behavior of recycled aggregate concrete filled stainless steel tubes (RAC-FSST). Constr Build Mater 2021;313:125532. https://doi.org/10.1016/j.conbuildmat.2021.125532.
[21] Han L-H, Xu C-Y, Hou C. Axial compression and bond behaviour of recycled aggregate concrete-filled stainless steel tubular stub columns. Eng Struct 2022;262:114306. https://doi.org/10.1016/j.engstruct.2022.114306.
[22] Xu C-Y, Han L-H, Hou C. Behaviour of recycled aggregate concrete-filled stainless steel tubular columns subjected to lateral monotonic and cyclic loading. Eng Struct 2023;293:116663. https://doi.org/10.1016/j.engstruct.2023.116663.
[23] B. S. I. (BSI). Stainless steels. Technical delivery conditions for bars, rods, wire, sections and bright products of corrosion resisting steels for construction purposes. London: British Standards Institution (BSI); 2009.
[24] Smith M. ABAQUS/standard user's manual, version 6.9.. Providence, RI: Dassault Systèmes Simulia Corp; 2009.
[25] B. S. I. (BSI). Eurocode 4. Design of composite steel and concrete structures. General rules and rules for buildings. British Standards Institution (BSI); 2005.